Experiments in Fluids (2018) 59:137
https://doi.org/10.1007/s00348-018-2591-3

RESEARCH ARTICLE

Quantification of airborne odor plumes using planar laser-induced fluorescence

Erin G. Connor[1] · Margaret K. McHugh[1] · John P. Crimaldi[1]

Received: 26 April 2018 / Revised: 15 June 2018 / Accepted: 9 July 2018

Abstract

Planar laser-induced fluorescence (PLIF) is used to quantify spatiotemporal structure of gaseous scalar plumes (Sc ≈ 1.5) in a benchtop-scale low-speed wind tunnel. The study is motivated by a desire to understand variations in information content in odor plumes used by animals for navigation. Acetone vapor is used as a fluorescent odor surrogate and is released isokinetically to form a neutrally buoyant plume. Three cases are investigated: a near-bed scalar release at 10 cm/s, a freestream scalar release at 10 cm/s, and a second freestream scalar release at 20 cm/s. PLIF image data are collected at 15 Hz and processed to provide distributions of instantaneous concentrations. Spatial distributions of mean concentration, root-mean-square fluctuations, and concentration intermittency are presented, along with probability density functions of concentrations at select locations. The results demonstrate significant differences in spatiotemporal structure of the scalar plumes across the three tested cases. In particular, the near-bed plume is markedly different from those released in the freestream. The results have important implications for understanding gaseous plume structure. Specifically, the results suggest that different flow and release conditions control constraints and opportunities for animals using odor plumes for navigational purposes.

Graphical abstract

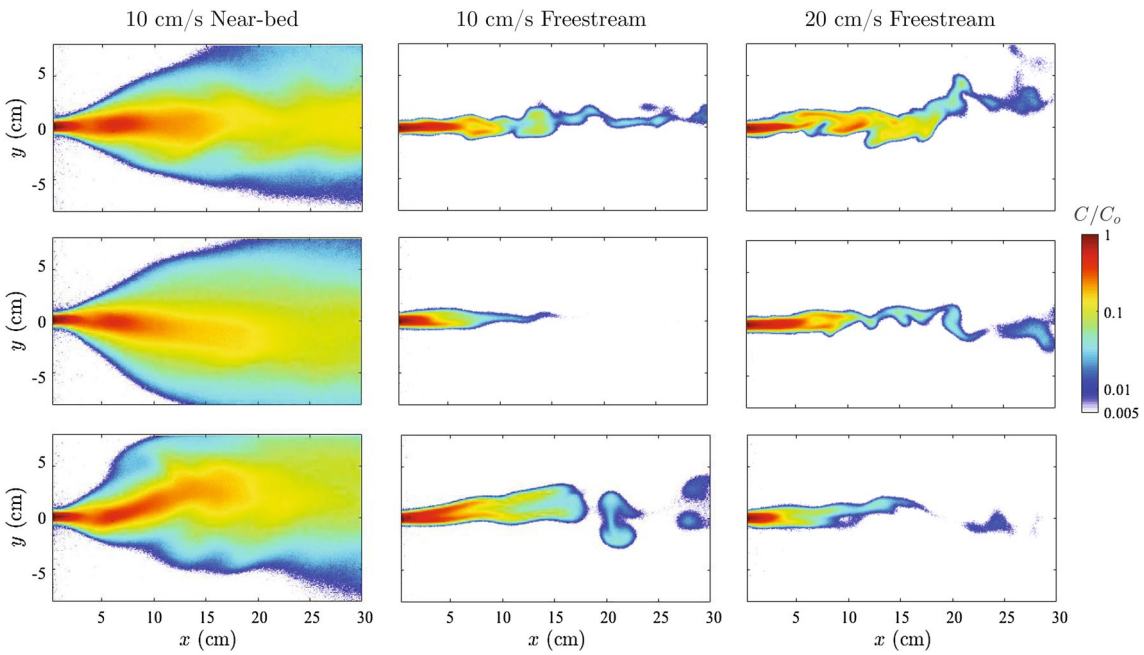

Extended author information available on the last page of the article

Published online: 04 August 2018

1 Introduction

High resolution spatial and temporal maps of chemical plumes inform our understanding of the dynamics of scalar quantities (mass or heat) in complex fluid environments. Plume dynamics dictate the dispersion of natural and anthropogenic emissions into the environment. In the context of biology and ecology, atmospheric and oceanic flows transport biochemical signals that many animals use for foraging, mating, and avoiding predators. Chemical plumes elicit a variety of behavioral responses in aquatic and terrestrial organisms that have evolved to navigate using olfaction. A first step towards understanding the biological processes involved is quantifying the spatial and temporal information carried by these plumes.

Scalar plumes that develop in turbulent flows exhibit complex spatiotemporal structure characterized by unsteady and intermittent concentration fields. When averaged over sufficiently long times, the mean plume distribution becomes smooth and easily described. In the context of animal navigation in odor plumes, however, animals typically only have access to information contained in the instantaneous plume structure; animal behavioral timescales are short compared to the timescales required to estimate the mean plume features (Webster and Weissburg 2001). It is, therefore, hypothesized (e.g., Ache and Young 2005) that animals use odor information contained in the instantaneous spatiotemporal scalar plume structure for navigational purposes.

The structure of neutrally buoyant scalar plumes in air has been previously measured in the laboratory and field using photoionization detectors (PID) that can detect a variety of volatile organic compounds. PID is very sensitive (typical detection limit < 1 ppm), and reasonably fast (typical frequency response $> 10^2$ Hz), enabling analysis of the temporal structure at a single point in the plume. Field studies of odor plume structure using PID show markedly different temporal scalar fluctuations under different environmental conditions (e.g., open field vs forrest, Murlis et al. 2000), and distance from the source (Yee et al. 1993). Laboratory studies using PID in a wind tunnel demonstrate sensitivity of scalar temporal structure to release condition (continuous vs pulsed) and flow type (uniform vs oscillatory) (Justus et al. 2002). However, the PID approach has several drawbacks: the invasive presence of a physical sensor in the flow can alter the ambient scalar structure, and a single PID sensor is only able to measure scalar structure at a single point at a time. These limitations motivate the value of full-field, non-invasive measurement techniques for measuring scalar plume structure.

Full-field, non-invasive, spatiotemporal measurements of neutrally buoyant scalar fields in turbulent flows have been largely confined to laboratory experiments in water using planar laser-induced fluorescence (aqueous PLIF, see review by Crimaldi 2008). Scalar structure for plumes developing in turbulent boundary layer flows in open-channel flumes have been quantified for scalars released from diffusive sources at the bed (Crimaldi et al. 2002), and from isokinetic sources above the bed (Liao and Cowen 2002; Webster et al. 2003). Together with the airborne PID studies, the aqueous PLIF studies demonstrate a rich and varied range of spatiotemporal structure of odor plumes as quantified by metrics such as scalar variance and intermittency; these metrics are shown to vary significantly with longitudinal and lateral distance from the source location. These studies form a foundation for understanding the available information that may be used by animals for odor navigation.

Plumes developing in air and water are subject to identical physics and are governed by the same set of equations. The Navier-Stokes equations govern the motion of the fluid flow, whereas the advection-diffusion equations govern the resulting transport and dispersion of the scalar within that flow. Dimensionally, the difference between flow in air and water (at a given speed and scale) is due only to differing fluid densities and dynamic viscosities; the difference between scalar plumes in air and water is also due to differing molecular diffusivities for the given scalar in the given fluid. Non-dimensionally, these differences are captured by Reynolds and Schmidt (or Prandtl) numbers, where the Schmidt number, Sc, is the ratio of the diffusivity of the fluid momentum to scalar diffusivity. In general, scalars in water or other liquids are weakly diffusive ($Sc \sim 10^3$), but scalars in air or other gases are more strongly diffusive ($Sc \sim 1$). It is possible to match the Reynolds number of an airborne plume by doing an experiment using water, but it is not possible to also match the Schmidt number. Therefore, to obtain experimental knowledge about the dynamics of airborne scalar plumes, it is necessary to perform the experiments in air as opposed to water. Typically, this is done by adapting the PLIF techniques commonly used in water for use in air.

In their foundational work, Lozano et al. (1992) established acetone as an ideal fluorescent tracer for gaseous PLIF. Compared with other gaseous fluorophores, it is relatively safe, stable and inexpensive. It is highly volatile allowing it to be easily vaporized at sufficiently high concentrations for detection. Acetone also meets practical criteria for use as a fluorescent tracer species: it absorbs UV radiation over a broad spectrum (225–320 nm) and fluoresces (peaks at 445 and 480 nm) with a short lifetime (4 ns). Most importantly, at moderate temperature and pressure, the fluorescence intensity is nearly linear with partial pressure so that measured intensity easily translates to quantitative concentrations.

As a result of these advantages, acetone PLIF has become a common method for measurements of scalar structure. The breadth of topics utilizing acetone PLIF now spans a range of fields including combustion, supersonic flow phenomena, and microelectromechanical systems. For non-reacting and moderate to subsonic flows, acetone PLIF has proven effective in studying scalar transport in a variety of flow conditions. Using PLIF-based temperature measurements of buoyant plumes, Kearney and Reyes (2003) showed the importance of large-scale coherent structures in conditionally averaged temperature fields and temperature fluctuation fields. Many more studies have investigated scalar mixing in different kinds of turbulent shear flows. Compared to analogous experiments in water, mixing across two parallel streams exhibited similar evolution and scaling dependencies but with notable differences not previously observed: greater mixing rates due to the higher molecular diffusivity (Cetegen 2006), and a Reynolds number dependence for laminar flows (Pickett and Ghandhi 2001). Among the many explorations of jets (including pulsed, coaxial, planar, and in cross flow), acetone PLIF techniques have clarified formation mechanisms (Smith and Mungal 1998; Getsinger et al. 2014) as well as confirmed the correspondence of the formation phases and evolution to different mixing characteristics (Meyer et al. 1999; Gevorkyan et al. 2016; Kothnur and Clemens 2005). Multiple studies sought model validation for scalar mixing in turbulent shear at subgrid scales for jets (Schumaker and Driscoll 2012; Su and Clemens 2003), buoyancy driven plumes (O'Hern et al. 2005), and plumes in decaying turbulence with limited shear (Markides and Mastorakos 2006). All of these applications demonstrate that acetone PLIF is a powerful tool for providing direct experimental observations of scalar physics in a variety of flows at large and small scales.

We implement acetone PLIF to quantify neutrally buoyant scalar plumes in a low-speed benchtop wind tunnel. In an olfactory context, odor plumes are typically released without excess momentum relative to the surrounding flow. A simple experimental implementation of this is an isokinetic source condition where the scalar is released with the same momentum as the local mean flow. Such isokinetic releases have been previously used in studies of olfactory plume dynamics (e.g., Liao and Cowen 2002; Webster et al. 2003; Bara et al. 1992). In our study, we test two release locations: in the freestream, and near a solid boundary. We analyze the effect of scalar release location and flow speed on the resulting spatiotemporal plume structure. The results provide insight into the available information content that might be used by animals or autonomous technologies for navigating within airborne odor plumes.

2 Experimental methods

We measured dynamic scalar plumes in a small wind tunnel using PLIF (Fig. 1). A horizontal laser sheet excited acetone vapor fluorescence which was then imaged from above with a digital camera. Resulting images were post-processed to produce quantitative spatial and temporal concentration distributions.

Flow facility We conducted experiments in a low-speed benchtop wind tunnel with a flow-through design. The tunnel test section was 30 cm wide, 30 cm tall, and extended 100 cm in the direction of the flow. Ambient air entered through a bell-shaped contraction which reduced in size from 60 cm by 60 cm to 30 cm by 30 cm (4:1 area ratio). The downstream contraction tapered to a 5 cm by 5 cm cross section which housed a 12V fan driving the flow. A laser sheet entered the test section through a narrow slit along the length of the test section. A camera imaged a portion of the test section from above through a glass top. Immediately before entering the test section, air flowed through a turbulence grid with mesh size $m = 2.54$ cm and diameter $d = 0.635$ cm (m/d ratio of 4). Air exited the test section through a 15 cm thick piece of honeycomb which eliminated swirl from the fan. A fluorescent tracer (acetone) was released into the center of the test section, 10 cm downstream of the turbulence grid, through a $D = 0.953$ cm diameter tube aligned with the flow.

Acetone generation We generated acetone vapor by flowing a carrier gas through flasks partially filled with liquid acetone. Two flasks in series ensured acetone saturation in the carrier gas for maximum resulting fluorescent signal.

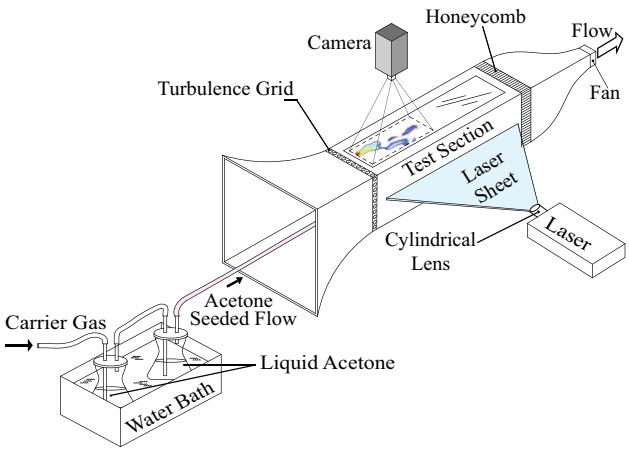

Fig. 1 Experimental schematic showing flow facility, acetone generation apparatus, and planar laser-induced fluorescence image acquisition system

To minimize fluctuations in acetone vapor concentration, flask temperature was controlled using a water bath at 19 °C, approximately 1 °C below ambient temperature. Because acetone vapor is denser than air, we generated the carrier gas by blending helium (41% v/v) and air (59% v/v). Mass flow controllers with a reported accuracy of 0.8 % regulated the mixing fraction of helium and air. Assuming a 95% seeding efficiency relative to saturation, the plume entering the tunnel was neutrally buoyant with a source concentration of approximately 25% acetone by volume. The molecular diffusivity of acetone in air at standard temperature and pressure is approximately 0.105 cm^2/s (Lugg 1968), resulting in Sc $\approx$ 1.5 for these experiments.

Planar laser-induced fluorescence We excited acetone vapor fluorescence in the test section using a Nd:YAG 532 nm pulsed laser equipped with a frequency doubling crystal. The laser output a 266 nm beam at 35 mJ/pulse and a frequency of 15 Hz. A dichroic mirror mounted directly on the laser head diverted residual 532 nm light. A cylindrical lens spread the beam into a 1 mm thick light sheet parallel to the test section floor. The light sheet was aligned with the tube delivering acetone to the center of the test section. Acetone plume fluorescence was imaged using a high-quantum-efficiency camera with 16-bit dynamic range and native resolution of 2048 × 2048. A 532 nm notch filter mounted on the lens blocked any stray 532 nm laser light present after the dichroic mirror. Additionally, we utilized 2 × 2 on-camera binning, the fastest available lens (*f*/0.95), and a completely dark environment to maximize signal-to-noise in the region of interest (ROI).

Image processing Normalized concentration distributions, C/C_o, were obtained from raw images, I_N, using a processing algorithm adapted from Crimaldi (2008):

$$\frac{C}{C_0} = \frac{1}{a_c}\frac{I_N - b}{B - b}, \tag{1}$$

where the calibration coefficient, a_c, was used to normalize the concentrations based on the source concentration at the tube exit. B is the distribution of light in the ROI captured by the camera with a constant and uniform acetone concentration; this distribution maps spatial variation in the light sheet intensity, as well as other non-uniformities due to lens vignette and pixel-to-pixel gain variations. The dark response of the camera, b, was obtained by averaging 500 images of the test section absent any acetone signal. It also corrected for stray light contamination present in the tunnel. Processed images were binned an additional 2 × 2 pixels resulting in a final 512 × 512 resolution (4 × 4 cumulative binning from the native camera resolution). The final pixel magnification was 0.74 mm/pixel, and a voxel corresponding to a physical volume of 0.55 mm^3. Signal dependent photon shot noise was the primary contributor to the root-mean-square (rms) noise of measured concentrations. As such, variations in the light sheet intensity also affected the signal-to-noise ratio which was higher where the light sheet was brighter and lower where the light sheet was dimmer. The maximum combined rms noise of the PLIF system in the absence of acetone fluorescence signal was equivalent to $0.001C_0$. For our results, we conservatively report a detectability limit equal to five times the rms noise floor ($0.005C_0$).

Flow conditions and data collection Three different experimental cases were used featuring different combinations of flow speeds and proximity to a boundary: near-bed at 10 cm/s, freestream at 10 cm/s, and freestream at 20 cm/s. In all experimental cases, the tunnel was operated with a mean flow speed matching the acetone flow speed for an isokinetic delivery. The two freestream cases featured delivery of acetone as far away from the test section top, bottom and sidewalls as possible. In the near-bed case, the centerline of the plume source was located 6 mm above a false floor that spanned the length and width of the test section. The height of the near-bed measurements corresponds to approximately 2 viscous wall units ($zu_\tau/\nu \approx 2$, where the shear velocity u_τ is estimated as 5% of the 10 cm/s freestream velocity), meaning that plume development takes place well within the viscous sublayer (VSL), where flow is relatively laminar. For both the 10 cm/s cases, the Reynolds number based on the tube diameter and turbulence grid mesh size were $Re_D = 63$ and $Re_m = 168$, respectively. For the 20 cm/s case, the Reynolds number based on the tube diameter and turbulence grid mesh size were $Re_D = 126$ and $Re_m = 336$, respectively. Both of the 10 cm/s data sets were a total of 40 minutes in length (36,000 images each), and the 20 cm/s data set was a total of 20 min (18,000 images).

3 Results

The objective of this study was to use an acetone PLIF system to quantify spatiotemporal structure in airborne odor plumes, where the acetone fluorophore was a surrogate for a natural odor. To understand the effect of the presence of a solid boundary on plume development, we compared two cases at the same flow speed (10 cm/s), where one case ("near-bed") had a false floor placed 6 mm below the center of the odor tube, and the second case ("freestream") did not. To understand the effect of flow speed, we then repeated the freestream case for a second, faster flow speed of 20 cm/s. Single images from the acetone PLIF technique map the spatial structure of scalar concentrations at a single instant in time. Series of these images then reveal the temporal variation of scalar spatial structure.

Representative distributions of normalized instantaneous scalar structure from three non-consecutive instances in time are shown as rows in Fig. 2, where columns correspond to the 10 cm/s near-bed (left), 10 cm/s freestream (middle), and 20 cm/s freestream (right) cases. The scalar source is located at the origin; streamwise and lateral distances from the source are given by x and y, respectively. The color-scale is chosen so that it ranges from the mean source concentration ($C/C_0 = 1$) down to the detectability limit for our acetone PLIF system which is one-half of one percent of the source ($C/C_0 = 0.005$). Instantaneous concentrations above the detectability limit persist across the entire 30 cm streamwise field of view for all three cases. The scalar structure of the 10 cm/s near-bed case is markedly different from the two freestream cases due to the no-flux condition at the bed and the placement of the source within the VSL. The wall impedes downward scalar diffusive spreading, reduces upward turbulent mixing, and retards flow velocities in the streamwise direction. All three of these factors contribute to plume dynamics that are diffusion-dominated, with increased lateral plume spreading seen in the figure. By comparison, turbulent stirring shapes the instantaneous structure of the two freestream cases which exhibit more intermittency and patchiness.

Series of images, such as those shown in Fig. 2, can be used to construct scalar time histories. Representative 60-second time histories on the plume centerline at $x = 10$ cm are shown for each of the three cases in Fig. 3. In each panel, the local mean concentration is shown with a dashed line for reference. The time histories reinforce the structural differences previously noted between the flow cases in the instantaneous scalar distributions. For the 10 cm/s near-bed

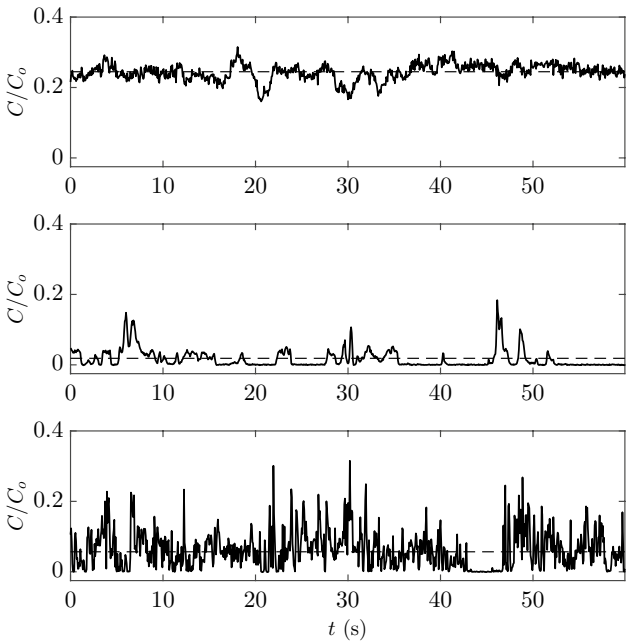

Fig. 3 Time histories of normalized centerline concentration at $x = 10$ cm for the near-bed case (top), freestream 10 cm/s case (middle), and freestream 20 cm/s case (bottom). In each panel, the dashed line indicates the local mean

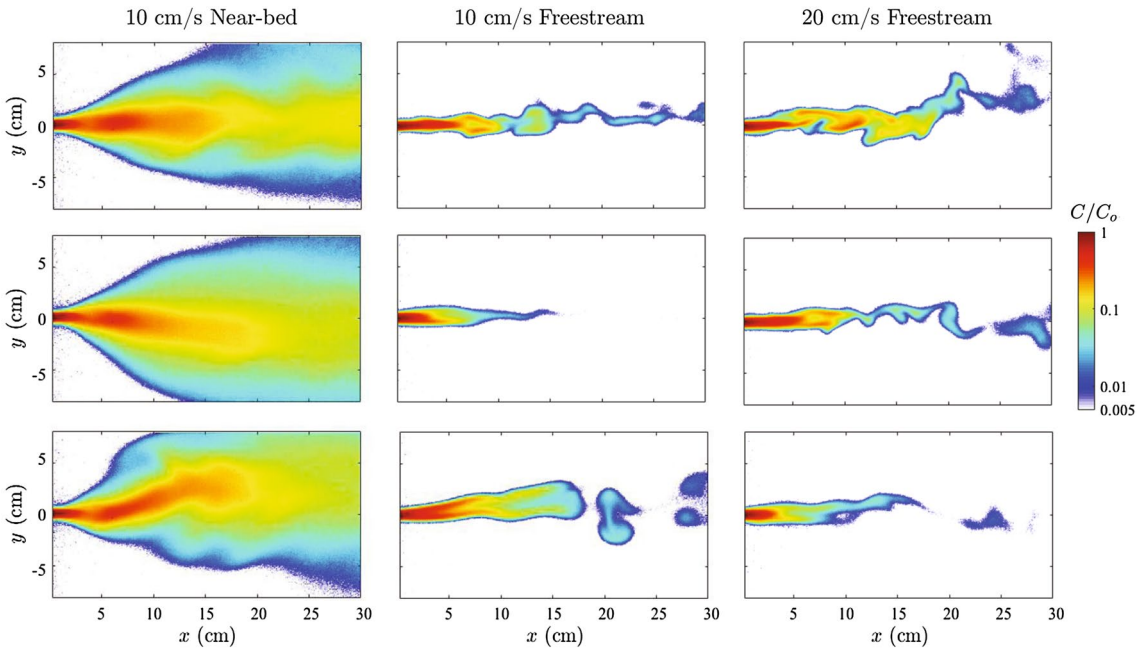

Fig. 2 Normalized instantaneous concentration distributions for each of the three flow cases (columns) for three representative instances in time (rows)

case (top), scalar concentrations at this location are always nonzero, and fluctuate above and below the mean with little skewness. Conversely, in both freestream cases (middle and bottom), the scalar concentrations are frequently zero and skewed with episodic fluctuations that extend well above the mean. The time histories further illustrate differences between the freestream cases. The 20 cm/s freestream case exhibits more energetic scalar fluctuations due to the increased strength of the turbulent flow field.

Mean scalar distributions computed as time-averages of series of instantaneous scalar distributions (36,000 images for the 10 cm/s cases, and 18,000 images for the 20 cm/s case) are shown in Fig. 4. Residual secondary circulations in the wind tunnel impart a slight lateral bias to the plumes in the positive y-direction. The secondary circulations likely result from room and wall effects outside the tunnel entrance, from the fan, and from flow incursions through the laser access slit. The mean distribution for the near-bed case (left column) is quite similar to each of the three corresponding instantaneous distributions (left column of Fig. 2), indicating the strongly persistent nature of plume structure within the VSL. These plumes clearly exhibit enhanced lateral spreading relative to the freestream cases. Mechanistically, the impermeability of the lower boundary obstructs scalar diffusion and dampens vertical mixing by the flow field. Additionally, the reduced streamwise velocities in the VSL are associated with a lower Péclet number (ratio of diffusive to advective timescales) allowing more diffusive spreading within a given streamwise advective distance. By contrast, the mean distributions of each of the two freestream cases (middle and right columns) show less resemblance to individual instantaneous distributions due to the highly intermittent nature of the plumes in the freestream turbulence. The faster 20 cm/s freestream plume persists farther downstream than the 10 cm/s freestream case. The higher flow speed has a corresponding higher Péclet number, resulting in decreased diffusive scalar mixing during the advective timescale associated with transport across the field of view. Therefore, it has larger $\overline{C}/C_o$ at a given x location compared to the 10 cm/s freestream case.

Normalized lateral profiles of mean concentration (symbols in Fig. 5) display Gaussian behavior at a range of streamwise locations within the plume. Profiles are normalized by the local centerline concentration and a standard deviation obtained by a fit to a Gaussian $\overline{C}/C_{\max} = \exp(-y^2/2\sigma^2)$ (solid lines in Fig. 5). For clarity, profiles were centered about $y/\sigma = 0$ based on the peak and binned an additional 2 pixels laterally (1.5 mm) and 7 pixels longitudinally (5.2 mm) prior to normalization. This centering process removes any lateral plume bias seen in Fig. 4. The self-similarity and lack of skewness across the field of view provide evidence that the acetone PLIF system used in

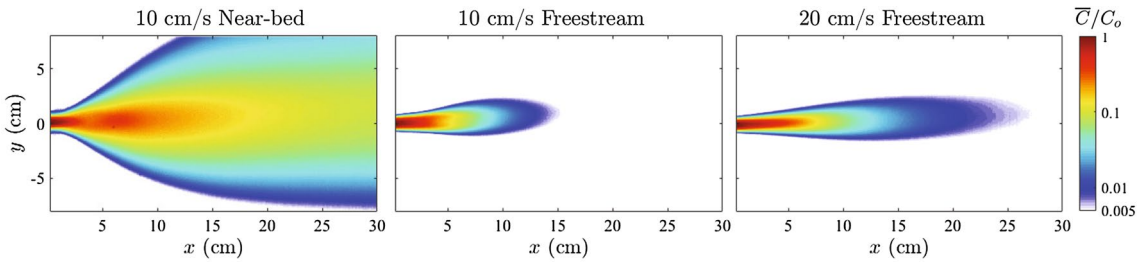

Fig. 4 Normalized mean concentration distributions for each of the three flow cases

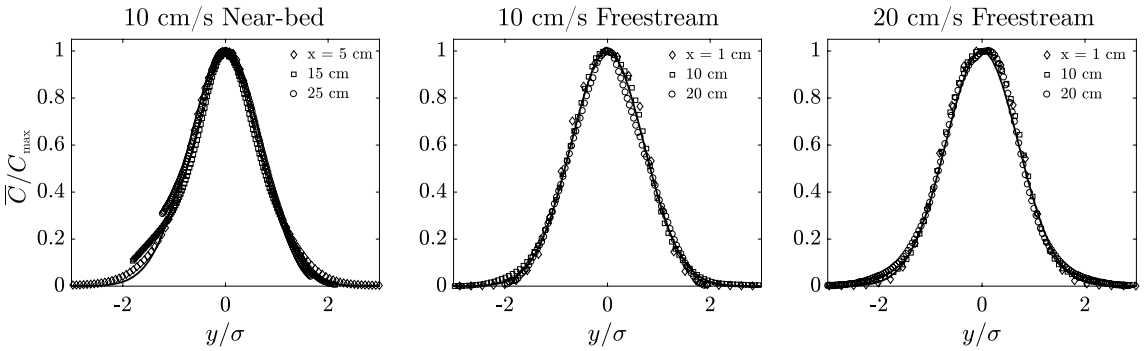

Fig. 5 Lateral profiles of normalized mean concentration at $x = 5$, 15, and 25 cm for the near-bed case (left), and at $x = 1$, 10, and 20 cm for each of the freestream cases (middle and right). Data are normalized via a fit to a Gaussian curve (solid line)

the study does not suffer from systematic bias due to laser absorption or light sheet variation.

Spatial distributions of root-mean-square (rms) scalar fluctuations, c', normalized by the source concentration, C_0, for each case are shown in Fig. 6. The rms distribution is characterized by bimodal lateral profiles (Fig. 7), consistent with several previous plume studies (e.g., Rahman and Webster 2005; Bara et al. 1992; Fackrell and Robins 1982). Off-center rms maxima likely arise when the length scale of a well-mixed central core is comparable to or larger than the local scale of plume meandering. For the present study, we release a well-mixed scalar stream of finite width ($D = 0.953$ cm). In the near-field, small scale meander motions produce peripheral rms maxima with an associated bimodal distribution. Further downstream ($x/D \gtrsim 10$), the meandering grows larger than the local scale of well-mixed regions. This acts to smooth out the peripheral peaks in the rms distribution. Although we were unable to measure sufficiently far downstream, we hypothesize that the rms distribution reverts to a unimodal shape. Because scalar fluctuations contribute nonlinearly to the rms calculation, the rms distributions extend farther laterally and longitudinally than the corresponding mean distributions for all cases. These peripheral regions of the plume are characterized by rare but still relatively strong scalar events; the intermittent nature of these events cause the mean distribution to decay spatially to zero more rapidly than the rms distribution.

In the context of odor plume navigation, it is useful to quantify the probability of encountering odor information at a given location. The intermittency factor γ (e.g., Wilson et al. 1985) is defined as the fraction of time concentrations are above a chosen threshold,

$$\gamma = \text{prob}[C \geq C_{\text{T}}]. \tag{2}$$

By definition, the intermittency factor is bounded as $0 \leq \gamma \leq 1$ and is high when concentrations are persistently above the threshold. Computed contours of intermittency factor are shown in Fig. 8, where we have used the detectability limit of the acetone PLIF system for the threshold value ($C_{\text{T}} = 0.005C_0$). For the near-bed case, γ contours spread rapidly in the lateral direction and persist far downstream. As an example, the $\gamma = 0.9$ contour (which envelops the region where $C \geq C_T$ 90% of the time) spans nearly the entire width of the imaged area at the downstream edge. Concentration dynamics within this region of large γ are consistent with the temporal structure exhibited in the representative time history (Fig. 3, top) where concentrations remain persistently above the threshold due to a relatively high mean and low rms. By comparison, γ contours for the freestream cases are much more spatially confined, and the probability of concentrations exceeding the threshold

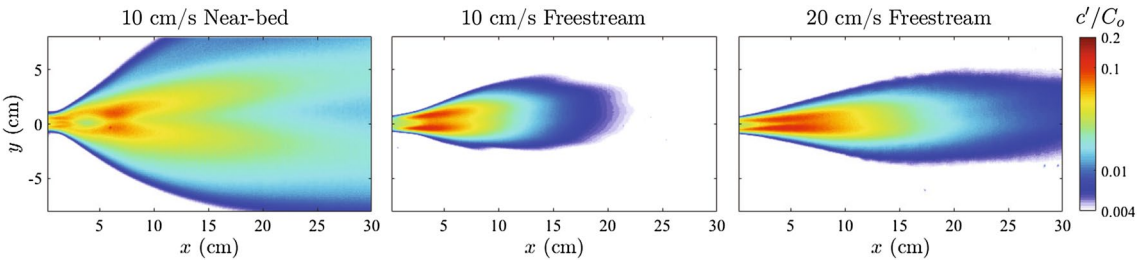

Fig. 6 Normalized root-mean-square concentration distributions for each of the three flow cases

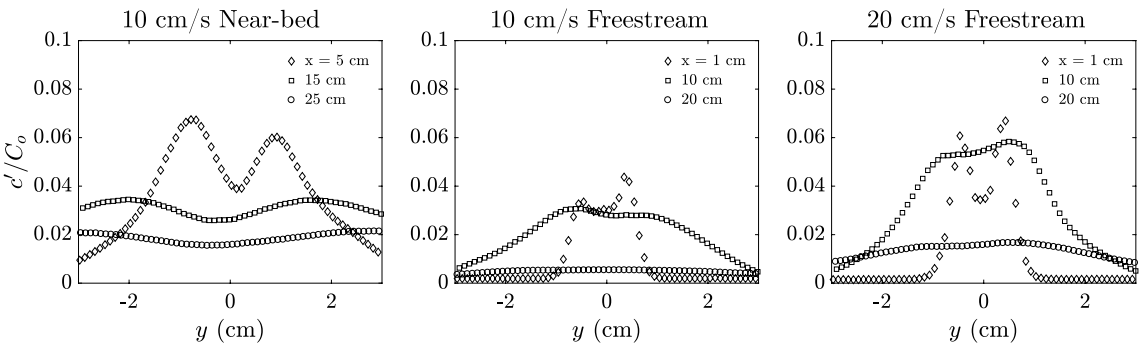

Fig. 7 Lateral profiles of normalized root-mean-square concentration for each of the flow cases. Streamwise locations shown are identical to Fig. 5

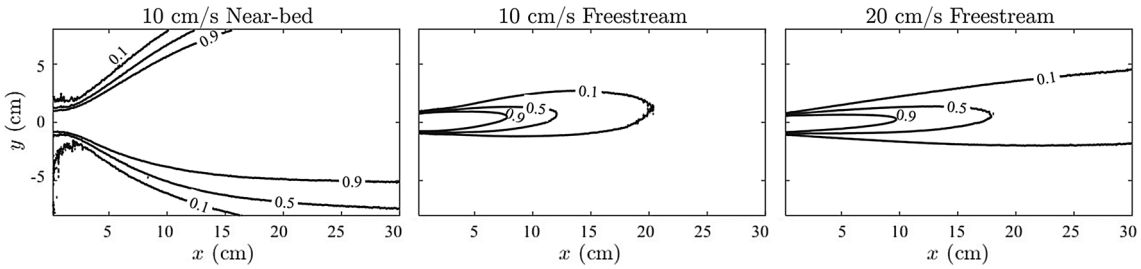

Fig. 8 Contours of intermittency factor each of the three flow cases

at any particular location is reduced relative to the near-bed case. The lower γ values in the freestream plumes are consistent with their representative time histories in Fig. 3 where concentrations are often zero and the mean is small, but relatively large episodic fluctuations occasionally drive the concentration above the threshold. Similar to the mean plume structure, γ contours extend farther downstream for the faster of the two freestream cases due to the reduced impact of dilution from molecular diffusion at the higher Péclet number.

Another useful perspective on odor dynamics relevant to navigation is the range and likelihood of scalar concentrations at given location. We calculated probability density functions (pdf) of normalized scalar concentrations at six locations for each of the three flow cases (Figs. 9, 10, 11). Streamwise locations in the pdfs (columns) correspond to those used in Figs. 5, 7, and each is shown both on and off the centerline (rows). Off the centerline and closest to the source (bottom left in each pdf array), the spike at $C/C_0 = 0$ confirms that this location is outside the extent of the plume in all three cases. The near-bed case pdfs (Fig. 9) differ from the two freestream cases in shape and spatial evolution away from the source. The negatively skewed shape of the near-bed pdfs results from the combined effects of small-scale molecular diffusion and larger scale plume meandering. Diffusion limits the highest possible concentrations at a downstream location producing sharp attenuation of the right side of the near-bed pdfs. At the same time, plume meandering and turbulence cause occasional incursions of low scalar concentration events to occur, producing a more gradual attenuation of the left side of the pdfs. As the plume advects downstream, the shape of the near-bed pdf changes very little but shifts to lower concentrations as scalar mixing dilutes the plume. Nonzero concentrations are still more likely due to plume homogenization in the VSL. By comparison, the pdfs for the freestream cases (Figs. 10, 11) change shape

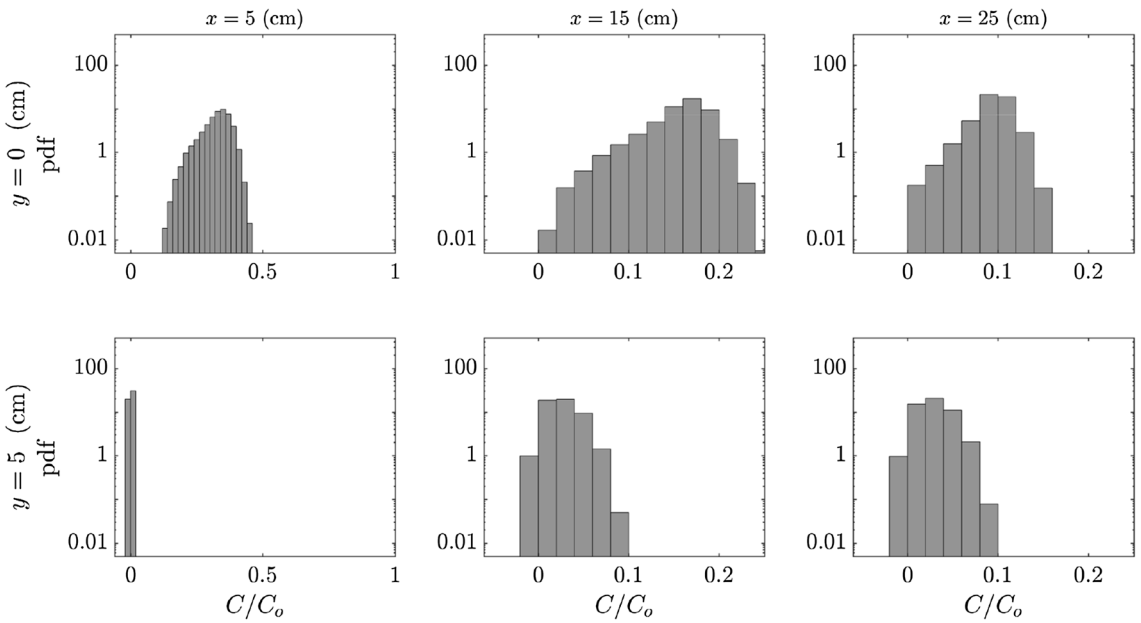

Fig. 9 Probability density functions of scalar concentration at select x and y locations for the 10 cm/s near-bed case

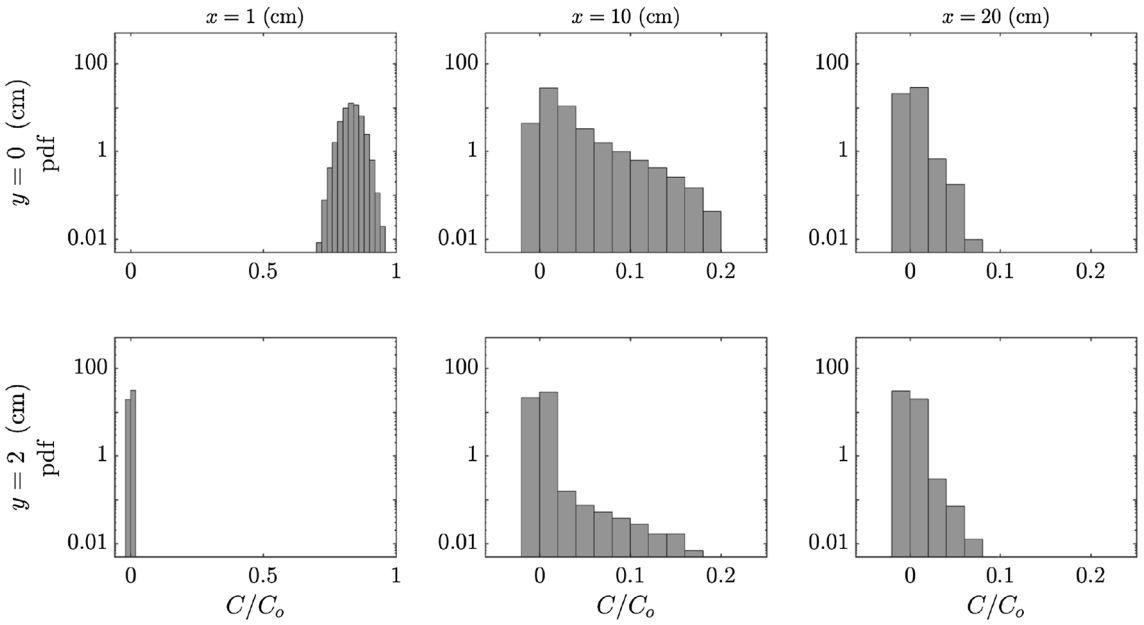

Fig. 10 Probability density functions of scalar concentration at select x and y locations for the 10 cm/s freestream case

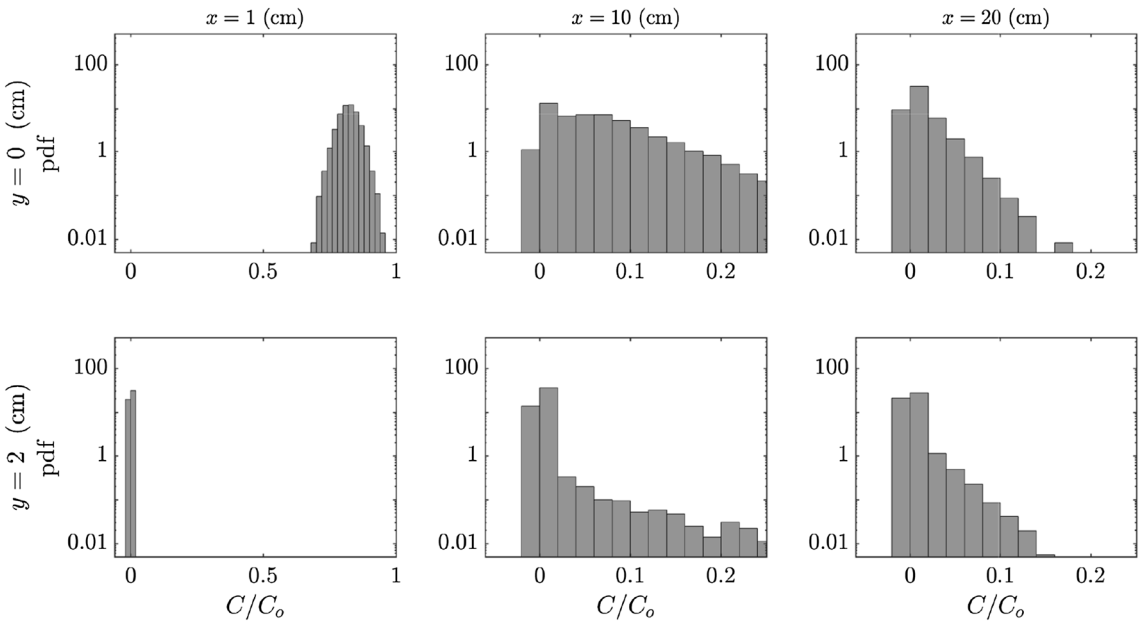

Fig. 11 Probability density functions of scalar concentration at select x and y locations for the 20 cm/s freestream case

dramatically across the plume. Close to the source (top left), the peak of the pdf is just below the source concentration. Farther downstream (top middle), three-dimensional turbulent dilution rapidly shifts the peak towards $C/C_0 = 0$. The large positive skew is directly related to the highly intermittent nature of the freestream cases; most of the time, at a given location, concentrations are near zero until a high concentration filament advects past. When considering pdfs relevant to animal navigation, Fackrell and Robins (1982) found similar exponential-like decaying distributions interpreted to result from rapid small-scale mixing and a complex "wispy" structure. This interpretation is visually consistent with the instantaneous plume images (Fig. 2) as well as the rms concentration distributions (Fig. 6). This trend appears typical for turbulent plumes as similar experiments carried out in water (e.g. Webster and Weissburg 2001) also had

highly skewed concentration pdfs owing to large intermittency. Moving away from the source, either longitudinally or laterally, the peak scalar concentration of filaments decreases, thus attenuating the tail of the pdfs and homogenizing the plume statistics laterally. Comparing the 10 cm/s freestream case to the 20 cm/s freestream case, the pdf characteristics are notably similar. The higher Péclet number simply increases the likelihood of higher concentrations at a given location. Were a searching agent to use the characteristics of the pdf to gain information about the source location, the changes in pdf shape may indicate location by skewness and strength of the maximum fluctuation.

4 Summary

Gaseous scalar plumes with Sc $\approx$ 1.5 were analyzed using an acetone PLIF system. Scalar releases were isokinetic, and neutral buoyancy was achieved by blending helium and air to balance the density of acetone. The three test cases explored were a near-bed release at 10 cm/s, a freestream release at 10 cm/s, and a freestream release at 20 cm/s. Image data collected at 15 Hz spanned a 16 cm by 30 cm field of view with a 0.74 mm/pixel resolution. Resulting distributions of normalized concentration had an estimated noise threshold and detectability limit of 0.1 and 0.5% of the maximum signal, respectively. Cross-stream profiles of mean concentration for all three cases exhibit symmetry and self-similarity as expected. Spatial distributions of mean and rms concentrations differ significantly among the three cases as a result of the underlying physical mechanisms for plume spreading and mixing. The near-bed case, residing within the VSL, spreads rapidly and maintains high concentrations with small relative fluctuations throughout the field of view. Comparatively, the freestream cases are subject to a more diffusive regime, and they have limited spatial extent as mean concentrations are rapidly diluted away from the source. The 20 cm/s case is distinct from the 10 cm/s case being characterized by more energetic fluctuations and higher concentrations at a given distance from the source due to its higher Péclet number.

In addition to mean and rms quantities, distributions of the intermittency factor and location-specific pdfs were analyzed by virtue of their pertinence to odor navigation. Again, the near-bed case stands apart from the other two cases as inherently different. The near-bed case has everywhere a higher γ owing to the persistence of nonzero scalar concentrations in the plume. Furthermore, there is little spatial variation in the pdf structures due to the homogeneity in the plume. The freestream cases have small γ, except very near the source, and positively skewed pdfs resulting from highly intermittent and patchy plume structure. These metrics offer insight into what a searching agent is likely to observe while navigating within a plume. If located within a VSL, the agent has the advantage of a greater and more continuous signal, but possibly less spatial information available in observed concentration variations (either in space or time). The intermittent and sporadic nature of the freestream plume creates obvious challenges for the task of locating the odor source, but also opportunities when considering the information available in concentration distributions. Animals using odor plumes for a variety of tasks likely exploit this spatiotemporal information now accessible experimentally via PLIF techniques.

Acknowledgements This work was supported by the National Science Foundation (USA), under Grant No. PHY 155586 to JPC

References

Ache BW, Young JM (2005) Olfaction: diverse species, conserved principles. Neuron 48:417–430

Bara BM, Wilson DJ, Zelt BW (1992) Concentration fluctuation profiles from a water channel simulation of a ground-level release. Atmos Environ 26A(6):1053–1062

Cetegen BM (2006) Scalar mixing in the field of a gaseous laminar line vortex. Exp Fluids 40:967–976

Crimaldi JP (2008) Planar laser induced fluorescence in aqueous flows. Exp Fluids 44:851–863

Crimaldi JP, Wiley MB, Koseff JR (2002) The relationship between mean and instantaneous structure in turbulent passive scalar plumes. J Turbul 3(014):1–24

Fackrell JE, Robins AG (1982) Concentration fluctuations and fluxes in plumes from point sources in a turbulent boundary layer. J Fluid Mech 117:1–26

Getsinger DR, Gevorkyan L, Smith OI, Karagozian AR (2014) Structural and stability characteristics of jets in crossflow. J Fluid Mech 760:342–367

Gevorkyan L, Shoji T, Getsinger DR, Smith OI, Karagozian AR (2016) Transverse jet mixing characteristics. J Fluid Mech 790:237–274

Justus KA, Murlis J, Jones C, Cardé RT (2002) Measurement of odor-plume structure in a wind tunnel using a photoionization detector and a tracer gas. Environ Fluid Mech 2:115–142

Kearney SP, Reyes FV (2003) Quantitative temperature imaging in gas-phase turbulent thermal convection by laser-induced fluorescence of acetone. Exp Fluids 34:87–97

Kothnur PS, Clemens NT (2005) Effects of unsteady strain rate on scalar dissipation structures in turbulent planar jets. Phys Fluids 17(125104):1–14

Liao Q, Cowen EA (2002) The information content of a scalar plume—a plume tracing perspective. Environ Fluid Mech 2:9–34

Lozano A, Yip B, Hanson RK (1992) Acetone: a tracer for concentration measurements in gaseous flows by planar laser-induced fluorescence. Exp Fluids 13:369–376

Lugg GA (1968) Diffusion coefficients of some organic and other vapors in air. Anal Chem 40(7):1072–1077

Markides CN, Mastorakos E (2006) Measurements of scalar dissipation in a turbulent plume with planar laser-induced fluorescence of acetone. Chem Eng Sci 61:2835–2842

Meyer TR, Dutton JC, Lucht RP (1999) Vortex interaction and mixing in a driven gaseous axisymmetric jet. Phys Fluids 11(11):3401–3415

Murlis J, Willis MA, Cardé RT (2000) Spatial and temporal structures of pheromone plumes in fields and forests. Physiol Entomol 25:211–222

O'Hern TJ, Weckman EJ, Gerhart AL, Tieszen SR, Schefer RW (2005) Experimental study of a turbulent buoyant helium plume. J Fluid Mech 544:143–171

Pickett LM, Ghandhi JB (2001) Passive scalar measurements in a planar mixing layer by PLIF of acetone. Exp Fluids 31:309–318

Rahman S, Webster DR (2005) The effect of bed roughness on scalar fluctuations in turbulent boundary layers. Exp Fluids 38:372–384

Schumaker SA, Driscoll JF (2012) Mixing properties of coaxial jets with large velocity ratios and large inverse density ratios. Phys Fluids 24(055101):1–21

Smith SH, Mungal MG (1998) Mixing, structure and scaling of the jet in crossflow. J Fluid Mech 357:83–122

Su LK, Clemens NT (2003) The structure of fine-scale scalar mixing in gas-phase planar turbulent jets. J Fluid Mech 488:1–29

Webster DR, Weissburg MJ (2001) Chemosensory guidance cues in a turbulent chemical odor plume. Limnol Oceanogr 46(5):1034–1047

Webster DR, Rahman S, Dasi LP (2003) Laser-induced fluorescence measurements of a turbulent plume. J Eng Mech 129(10):1130–1137

Wilson DJ, Robins AG, Fackrell JE (1985) Intermittency and conditionally-averaged concentration fluctuation statistics in plumes. Atmos Environ 19(7):1053–1064

Yee E, Kosteniuk PR, Chandler GM, Biltoft CA, Bowers JF (1993) Statistical characteristics of concentration fluctuations in dispersing plumes in the atmospheric surface layer. Bound Layer Meteorol 65:69–109

Affiliations

Erin G. Connor[1] · Margaret K. McHugh[1] · John P. Crimaldi[1]

✉ John P. Crimaldi
crimaldi@colorado.edu

[1] Department of Civil, Environmental and Architectural Engineering, University of Colorado, Boulder, CO 80309-0428, USA